Supporting Information for

Discovery of two predictable (3, 18)-connected topologies based on Wells-Dawson type cage for the design of porous metal phosphonocarboxylate frameworks

Wenyan Dan,[a] *Zhenxia Chen**[b], *Yun Ling*[b], *Yu Jia*[b], *Yongtai Yang*[b], *Xiaofeng Liu*[b] *and Mingli Deng*[b]

a. College of Chemical Science and Engineering, Tongji University, Shanghai 200092, China.

b. Shanghai Key Laboratory of Molecular Catalysis and Innovative Materials,

Department of Chemistry, Fudan University, Shanghai 200438, China.

e-mail: zhxchen@fudan.edu.cn.

Table of Contents

Structural description of MnPCF-1

MnPCF-1 crystallize in the trigonal space group of $R\bar{3}$. **MnPCF-1** has the same asymmetric unit with **CoPCF-1**. Mn1 is five-coordinated with three phosphonate oxygens, one carboxylate oxygen, and one DMF. Mn2 exhibits a six-coordination involving one hydroxyl group (μ_3-OH), two phosphonate oxygens, and three carboxylate oxygens. The Mn-O bonds span from 1.983 (6) to 2.306(6) Å. The structure features a rugby ball shaped unit with the formula of $Mn_{12}(\mu_3\text{-}OH)_2(CO_2)_{12}(PO_3)_6(DMF)_6$ with dimensions approximately 1.58 × 1.30 nm^2. The termini of this structure are capped by a $\{Mn_3(\mu_3\text{-}OH)\}$ equilateral triangle and three carboxylate groups, with the μ_3-OH group displaced by about 0.38(5) Å out of the $\{Mn_3\}$ plane. The intrametallic distance of Mn2···Mn2 is 3.598(2) Å. Each Mn2…Mn2 edge is bridged by a carboxylate group from the pbpdc ligand. The phosphonate group adopts the same coordination mode with **CoPCF-1**, binding two Mn1, two Mn2 in the same layer and one Mn1 from the adjacent layer. Another carboxylate group bridges Mn1 and Mn2 with a short distance of 3.229(2) Å. All carboxylate groups exhibit *syn-syn* coordination modes. Considering the $Mn_{12}(\mu_3\text{-}OH)_2(CO_2)_{12}(PO_3)_6(DMF)_6$ cluster as an 18-connected node, and the slightly twisted biphenyl group of $bpbdc^{4-}$ as a 3-connected node, the structure constitutes a rare 3D (3, 18)-connected open-framework with the **gez** topology like **CoPCF-1**.

Structural description of MnPCF-2

The asymmetric unit of **MnPCF-2** contains two Mn^{2+} ions, one protonated dimethylamine, 3/4 acetic acid, 1/12 protonated water, 1/3 μ_3-OH and one deprotonated $pbpdc^{4-}$. There are disordered guest molecules, which we removed from the final structure using SQUEEZE procedure of PLATON. **MnPCF-2** also features a rugby ball SBU with acetic acid as the coordinated terminal group. The dimensions of Mn_{12}SBU are around 1.36 × 1.13 nm^2, slightly smaller than that of **MnPCF-1**. The phosphonate group adopts the same coordination mode with **CoPCF-2**. Wells−Dawson type cages of **MnPCF-2** are further connected by the $bpbdc^{4-}$ ligands to form a 3-D structure. Considering the duodenary phosphonocarboxylate-based cluster from **MnPCF-2** as an 18-connected node, and $bpbdc^{4-}$ as a 3-connected node, the structure represents a (3, 18)-connected frameworks with **gea** topology.

Magnetic properties of CoPCF-2 and MnPCF-2.

In **CoPCF-2**, the value of $\chi_M T$ at 300 K is 14.82 $cm^3\ mol^{-1}\ K$ (Figure S15a), which is larger than the calculated spin-only value (11.22 $cm^3\ mol^{-1}\ K$) for six Co(II) ($S = {}^3/_2$, g=2.0) ions, indicating the orbital contribution from the high-spin octahedral Co(II). Upon cooling, $\chi_M T$ steadily decreases, suggesting significant antiferromagnetic exchange between the Co(II) ions connected through one μ_3-OH and O−C−O bridges. The intramolecular antiferromagnetic interaction is confirmed by the Curie−Weiss law above 15 K with C =16.16 $cm^3\ K\ mol^{-1}$ and θ = −21.72 K (Figure S15a), revealing dominant antiferromagnetic interactions between the Co(II) ions and the presence of spin-orbit couplings. The large Co1−O8−Co1 angles of 119.25(5)°, and the *syn−syn* bridging mode of the carboxylate group further support antiferromagnetic interactions.

The field dependence of magnetization of **CoPCF-2** at 2 K (Figure S16a) reveals a magnetization of 8.12 Nβ per Co_6 unit at an applied field of 70 kOe. This value, smaller than the high-spin Co(II) saturation (18 Nβ for six Co(II) ions), and the absence of a hysteresis loop suggest dominant antiferromagnetic coupling between Co(II) ions in **CoPCF-2**. The dM/dH plot (see Figure S17c) shown no characteristic of spin-flop behaviour in **CoPCF-2**.

The $\chi_M T$ and χ_M versus T plots of **MnPCF-2** (Figure S15b) exhibit a $\chi_M T$ value of 22.63 $cm^3\ mol^{-1}\ K$ at 300 K, lower than the calculated spin-only value (26.26 $cm^3\ mol^{-1}\ K$) for six Mn(II) ($S = {}^5/_2$, g=2.0) ions, indicating an orbital contribution from high-spin octahedral Mn(II). Above 15 K, the Curie−Weiss law fits well with C = 26.72 $cm^3\ K\ mol^{-1}$ and θ = −49.90 K (see Figure S15b), supporting antiferromagnetic interactions between the Mn(II) ions. As the temperature decreases, $\chi_M T$ achieve a minimum value of 0.7546 $cm^3\ mol^{-1}\ K$ at 2 K, indicating substantial antiferromagnetic exchange between Mn(II) ions connected through μ_3-OH and O−C−O bridges. The large Mn−O−Mn angle of 117.45(8)° as well as the *syn−syn* bridging mode of the carboxylate group, reinforce the presence of antiferromagnetic interactions. The field dependence of magnetization at 2 K (Figure. S16b) for **MnPCF-2** shows a magnetization of 4.89 Nβ per Mn_6 unit at an applied filed of 70 kOe. This value is lower than the saturation value of six Mn ions and no hysteresis loop is observed. The magnetization increases gradually with increasing external field and displays an inflexion at about 65 kOe, determined by the peak in the dM/dH plot (Figure S17d), showing a characteristic of spin-flop behaviour.

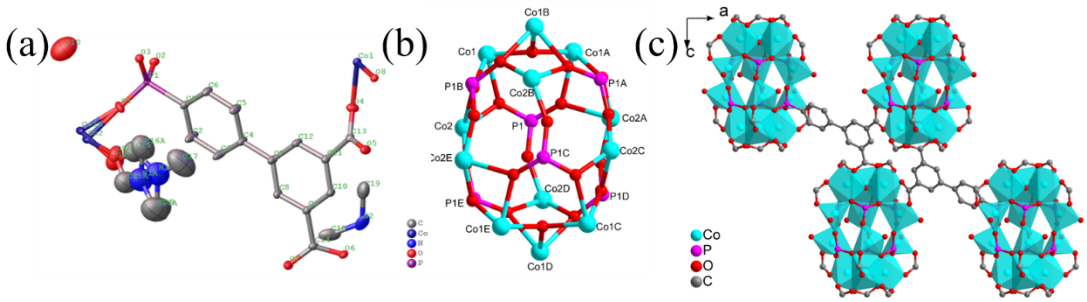

Figure S1 (a)The structural unit in **CoPCF-1**. (b) $\{Co_{12}P_6\}$ core of $Co_{12}(\mu_3\text{-}OH)_2(CO_2)_{12}(PO_3)_6(DMF)_6$ cluster. Symmetry code: A(-1-x+y, 1-x, z); B(1-y, 2+x-y, z); C(-x, 2-y, -z); D(-1+y, -x+y, -z); E(1+x-y, 1+x, -z). (c) each $pbpdc^{4-}$ linked by three Co_{12} clusters.

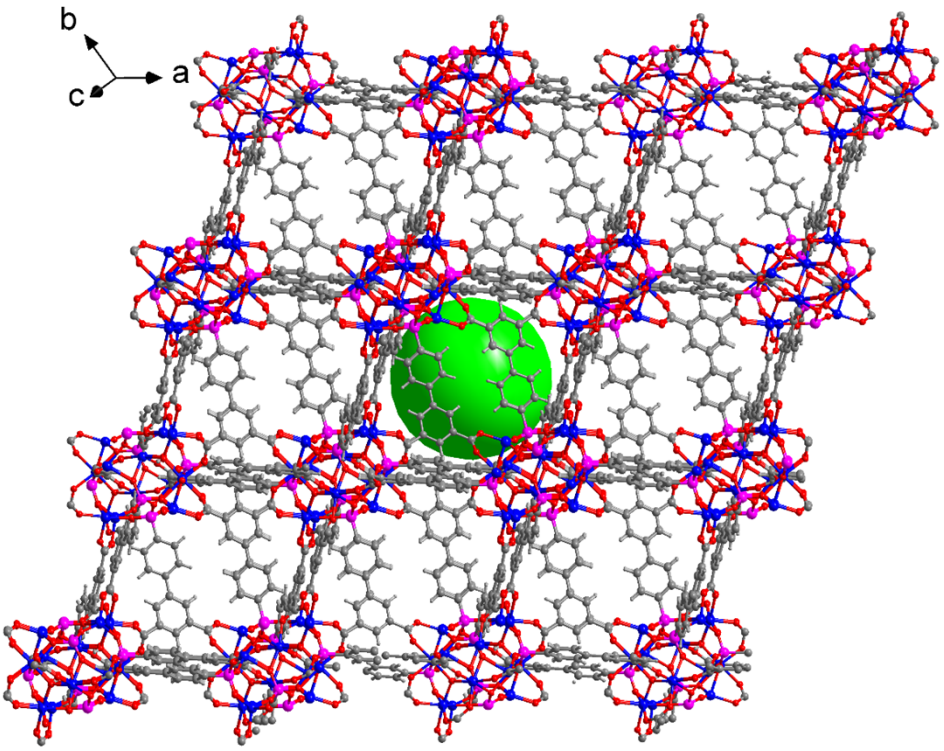

Figure S2 Packing view of **CoPCF-1** (green ball are added to highlight the quadrangular cage).

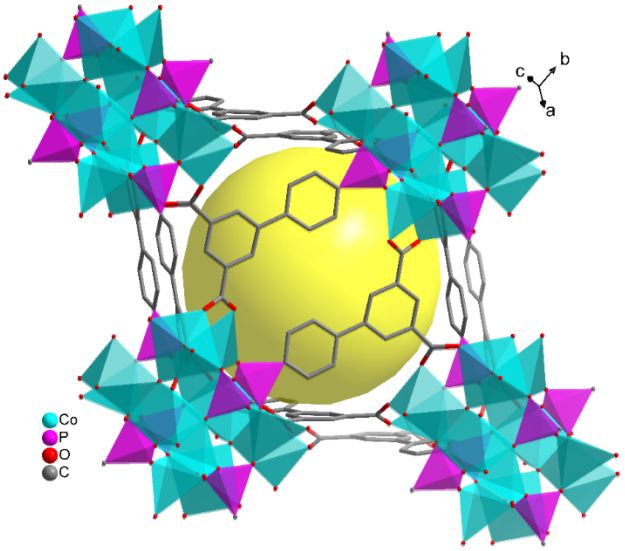

Figure S3 General view of **CoPCF-1** reveal a quadrangular cage (yellow ball are added to highlight the quadrangular cage).

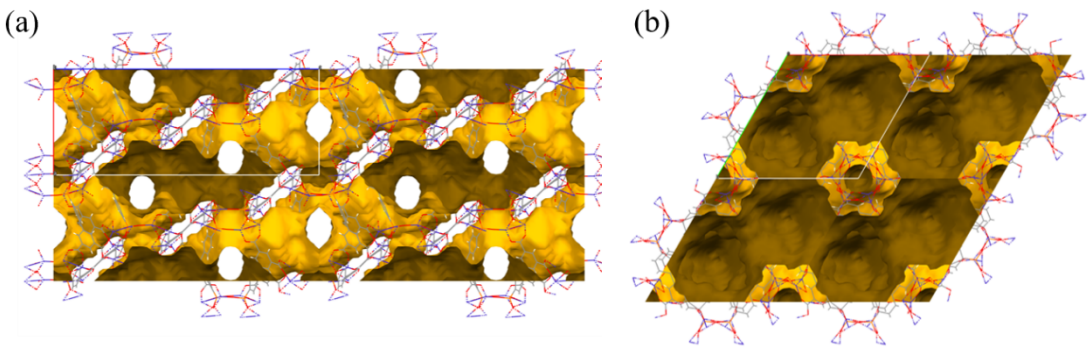

Figure S4 Connolly surface area calculated with probe atomic radii of 1.2 Å in **CoPCF-1a:**(a) along b axis, (b) along c axis.

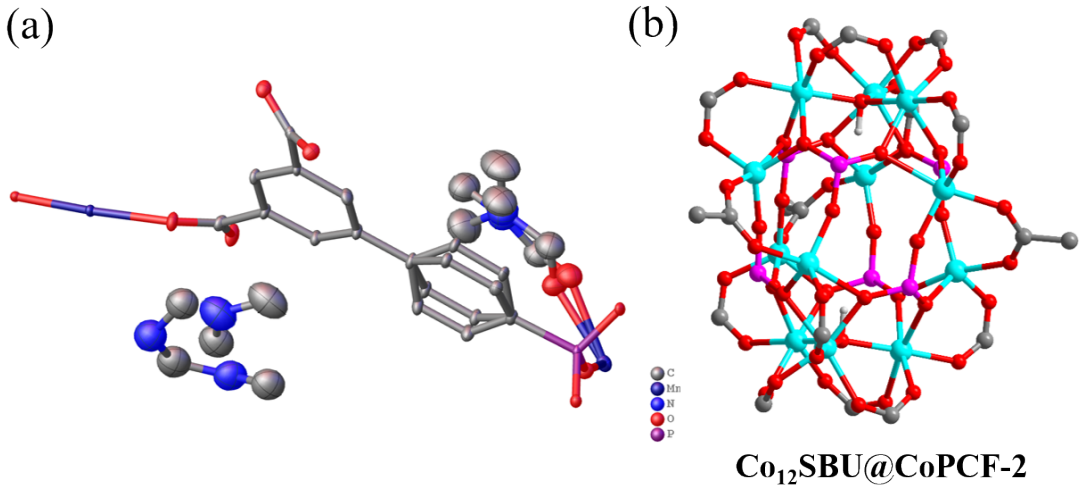

Figure S5 (a)The structural unit in **CoPCF-2** and (b) Co_{12} cluster in **CoPCF-2**.

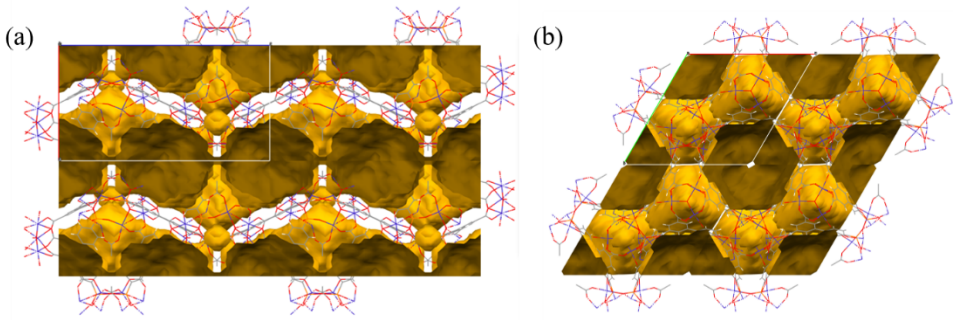

Figure S6 Connolly surface area calculated with probe atomic radii of 1.2 Å in **CoPCF-2**: (a) along b axis, (b) along c axis.

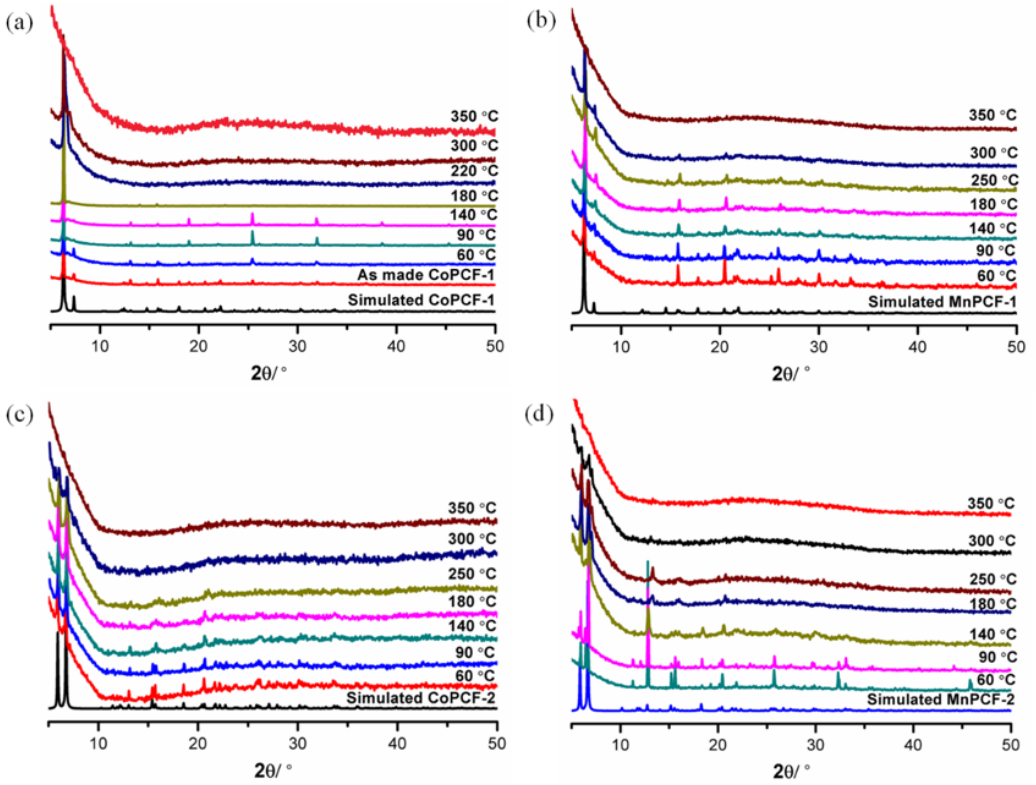

Figure S7 PXRD patterns of compounds in air from 60 °C temperature to 350 °C:(a) **CoPCF-1**; (b)**MnPCF-1**; (c) **CoPCF-2**; (d)**MnPCF-2**.

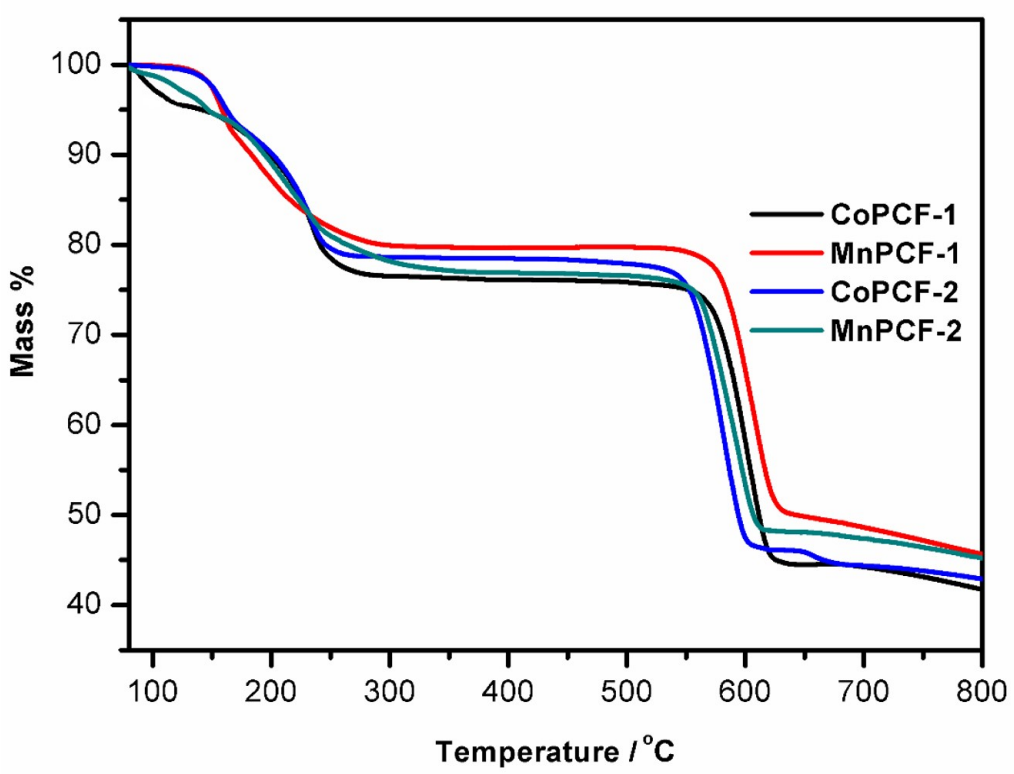

Figure S8 TGA curve of as-synthesized compounds.

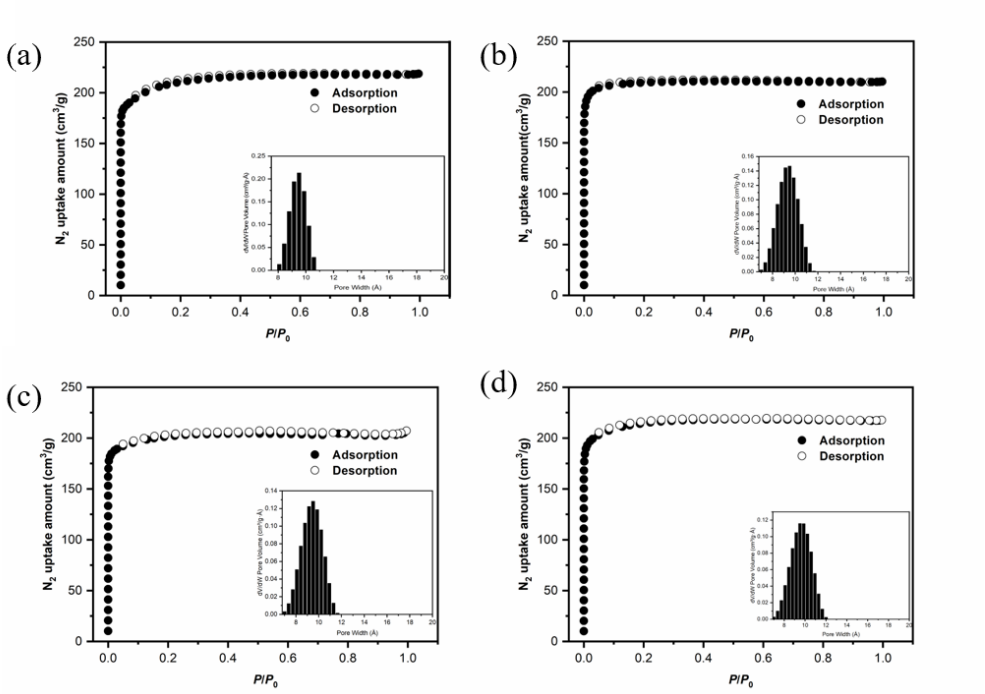

Figure S9 N_2 sorption isotherms of activated **MPCFs** at 77 K: (a) **CoPCF-1**, (b) **MnPCF-1**, (c) **CoPCF-2**, and (d) **MnPCF-2** (The inset graph indicates the pore size distribution.).

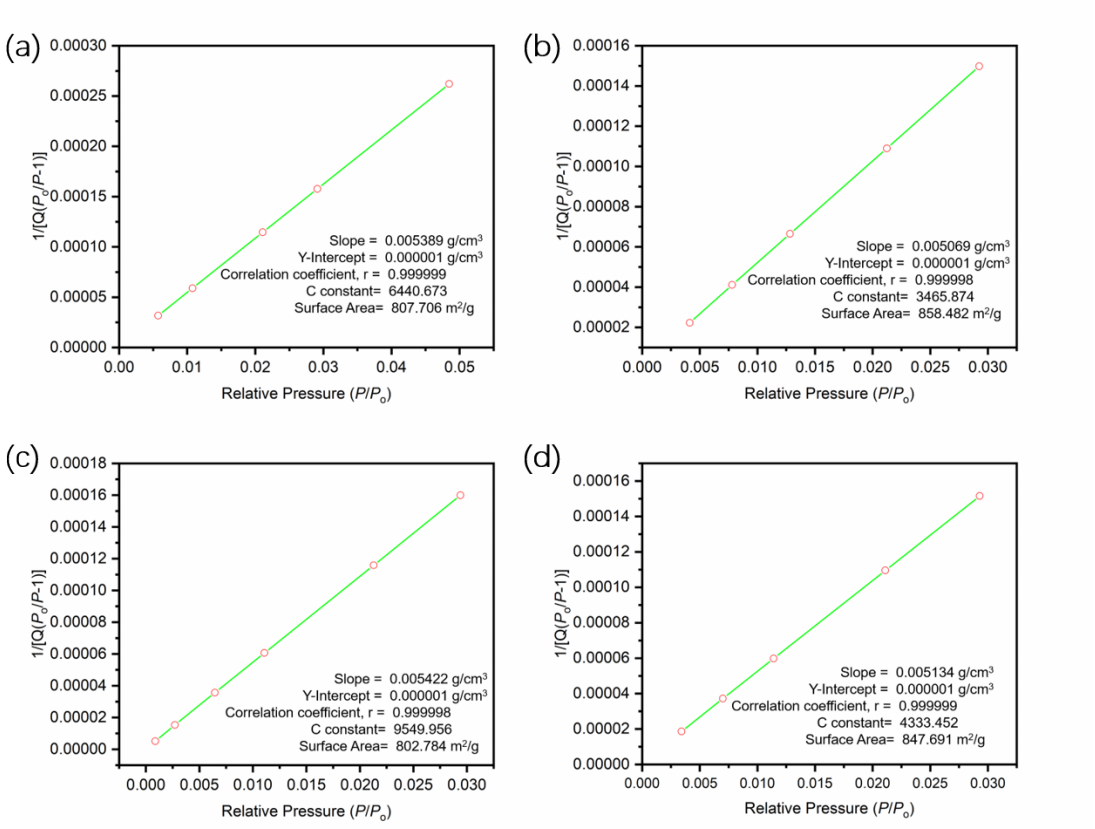

Figure S10 BET surface area plot for **MPCFs**: (a) **CoPCF-1**, (b) **MnPCF-1**, (c) **CoPCF-2**, and (d) **MnPCF-2**.

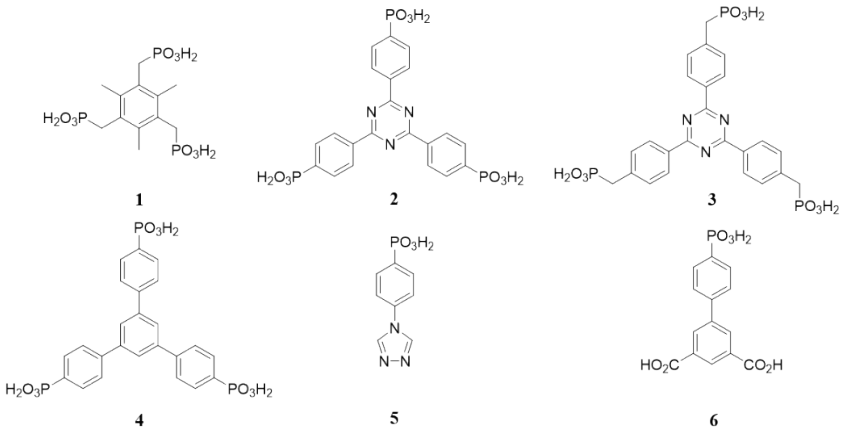

Figure S11 Phosphonate ligands employed for the synthesis of potentially porous MOFs.

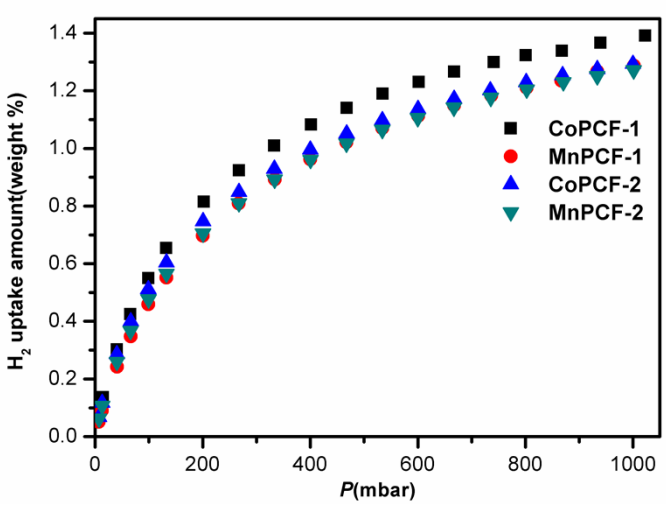

Figure S12 Hydrogen-sorption isotherms of **MPCFs** at 77 K: (a) **CoPCF-1**, (b) **MnPCF-1**, (c) **CoPCF-2**, and (d) **MnPCF-2**.

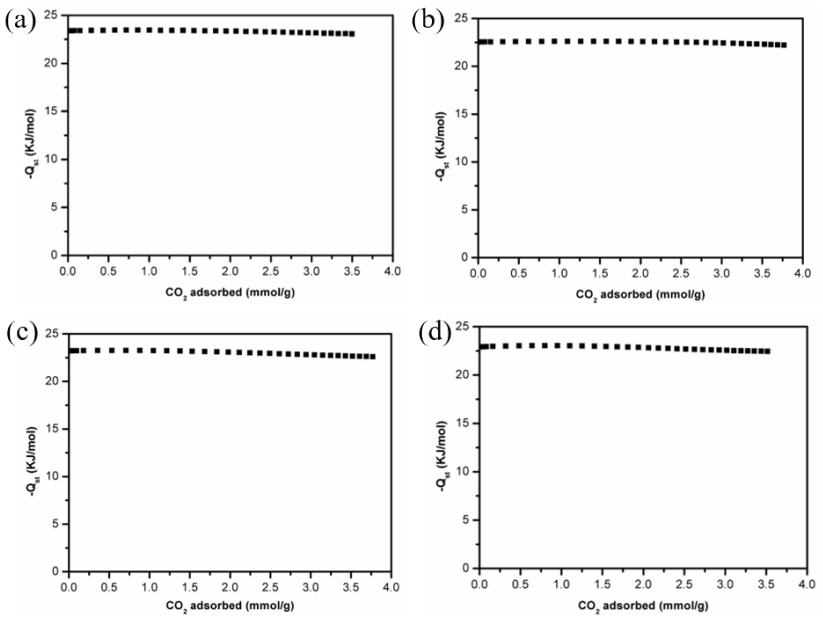

Figure S13 Isosteric heats of CO_2 adsorption for compounds:(a)**CoPCF-1**; (b)**MnPCF-1**; (c)**CoPCF-2**; (d)**MnPCF-2**.

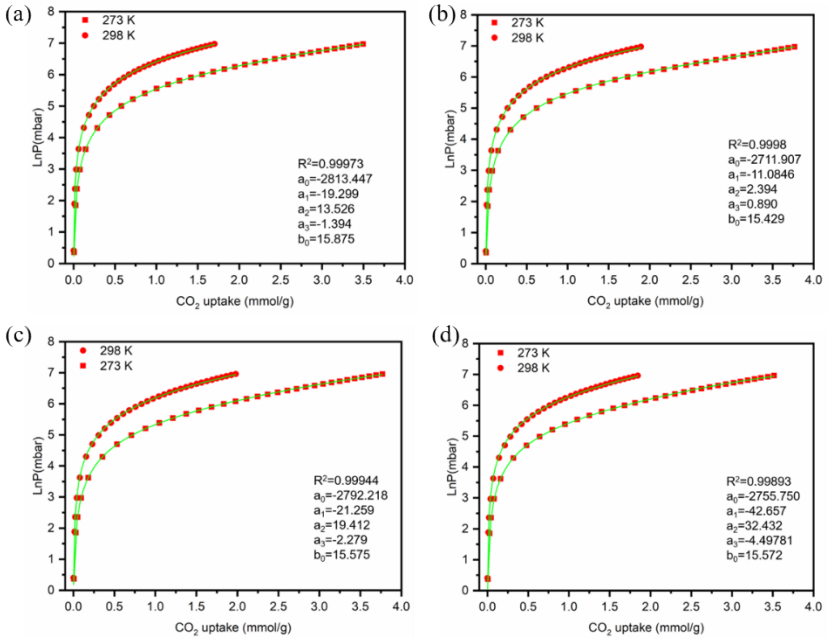

Figure S14 The CO_2 isotherms at 273 K and 298 K (symbols) and the Virial equation fits (lines) for **MPCFs**: (a)**CoPCF-1**; (b)**MnPCF-1**; (c)**CoPCF-2**; (d)**MnPCF-2**.

The adsorption selectivity for binary mixtures defined by equation 1.

$$S_{i/j} = \frac{x_i/x_j}{y_i/y_j} \quad (1)$$

where S is the selectivity factor, x_i represents the quantity adsorbed of component i, and y_i represents the partial pressure of component i. The selectivity calculation for CO_2 over N_2 is performed using the adsorption capacities at pressures of approximately 0.15 bar for CO_2 and 0.75 bar for N_2.

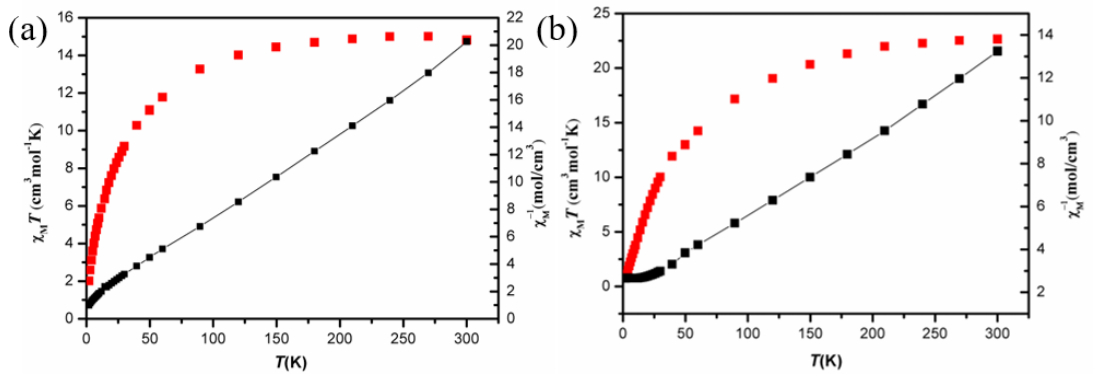

Figure S15 Temperature dependence of χ^{-1}_m and $\chi_m T$ for **CoPCF-2**(a) and **MnPCF-2**(b) under 2 kOe. The solid lines represent the fit of Curie-Weiss law.

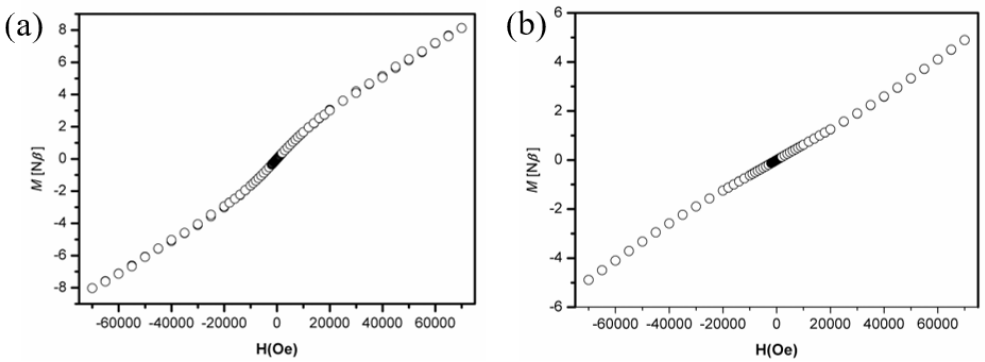

Figure S16 The isothermal magnetization curve for **CoPCF-2**(a) and **MnPCF-2**(b) at 2 K.

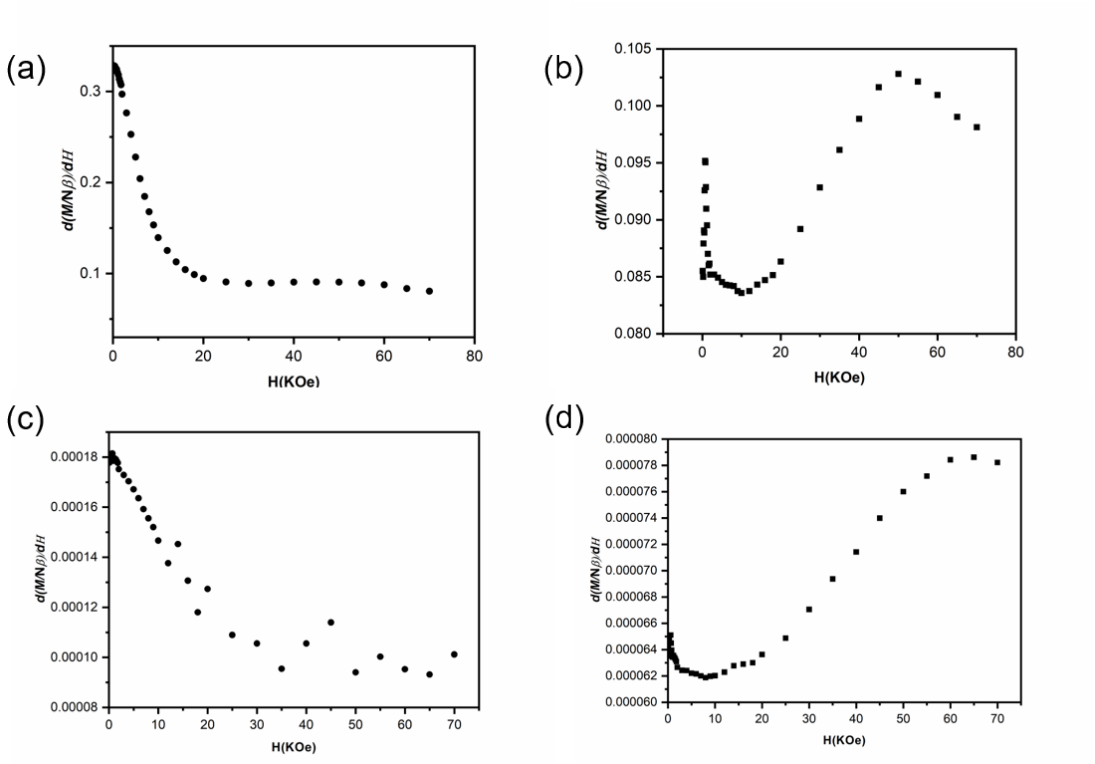

Figure S17 The d*M*/d*H* versus *H* curve for **CoPCF-1**(a), **MnPCF-1**(b), **CoPCF-2** and **MnPCF-2**(d) at 2 K.

Table S1 Selected bond lengths (Å) and angles (º) for **MPCFs**.

CoPCF-1			
Co1–O5$^{\#1}$	2.137(2)	Co1–Co2A$^{\#5}$	2.916(6)
Co1–O6$^{\#2}$	2.064(3)	Co2–O1	1.885(3)
Co1–O8	2.0440(11)	Co2–O7$^{\#6}$	1.951(3)
Co1–O2$^{\#3}$	2.195(2)	Co2–O2$^{\#7}$	1.984(3)
Co1–O3$^{\#4}$	2.180(2)	Co2–O3$^{\#8}$	2.307(3)
Co1–O4	2.021(3)	P1–O1	1.511(3)
O5–Co1–O2	168.93(9)	O3–Co1–O2	77.96(9)
O5–Co1–O3	109.16(10)	O4–Co1–O5	87.02(11)
O6–Co1–O2	90.03(10)	O4–Co1–O6	88.99(10)
O6–Co1–O2	90.03(10)	O4–Co1–O8	97.69(10)
O6–Co1–O3	88.67(9)	O4–Co1–O2	85.34(11)
O8–Co1–O5	97.27(11)	O4–Co1–O3	163.13(10)
O8–Co1–O6	173.22(9)	O1–Co2–O7	117.94(12)
O8–Co1–O2	91.69(10)	O1–Co2–O2	129.88(13)
O8–Co1–O3	85.27(10)	O1–Co2–O3	95.45(15)

Symmetry transformations used to generate equivalent atoms: #1: 1-Y, +X-Y, +Z; #2: 0.66667+X-Y, -0.66667+X, 1.33333-Z; #3: 1.66667-X, 1.33333-Y, 1.33333-Z; #4: 1.66667-Y, 0.33333+X-Y, 0.33333+Z; #5: 0.66667+Y, 1.33333-X+Y, 1.33333-Z; #6: 2-X, 1-Y, 1-Z; #7: +Y, 1-X+Y, 1-Z; #8: 1+X-Y, +X, 1-Z

MnPCF-1			
Mn1–O1	1.983(7)	Mn2–O3$^{\#5}$	2.306(6)
Mn1–O2$^{\#2}$	2.085(6)	Mn2–O4	2.114(6)
Mn1–O3$^{\#3}$	2.198(6)	Mn2–O6$^{\#6}$	2.201(6)
Mn1–O5$^{\#1}$	2.100(6)	Mn2–O7$^{\#7}$	2.113(6)
Mn1–O9	2.273(10)	Mn2–O8	2.113(2)
Mn2–O2$^{\#4}$	2.306(6)	P1–O1	1.520(7)
O1–Mn1–O2	134.4(3)	O9–Mn1–Mn2	123.2(3)
O1–Mn1–O3	100.9(2)	O2–Mn2–Mn1	40.04(14)
O1–Mn1–O5	114.5(3)	O2–Mn2–O3	75.4(2)
O1–Mn1–O9	92.2(3)	O3–Mn2–Mn1	42.87(14)
O2–Mn1–O3	82.4(2)	O4–Mn2–Mn1	67.13(18)
O2–Mn1–O5	110.9(3)	O4–Mn2–O2	87.3(2)

O2–Mn1–O9	93.8(3)	O4–Mn2–O3	85.9(2)
O3–Mn1–O9	165.0(3)	O4–Mn2–O6	85.6(2)
O5–Mn1–O3	90.7(2)	O6–Mn2–Mn1	141.83(18)
O5–Mn1–O9	77.1(3)	O6–Mn2–O2	169.1(2)

Symmetry transformations used to generate equivalent atoms: #1: 0.66667-X, 0.33333-Y, 1.33333-Z; #2: 0.66667+X-Y, 0.33333+X, 1.33333-Z; #3: -0.33333+Y, 0.33333-X+Y, 1.33333-Z; #4: -X+Y, -X, +Z; #5: 1-Y, +X-Y, +Z; #6: 1-X, -Y, 1-Z; #7: +Y, -X+Y, 1-Z

CoPCF-2

Co1–O5$^{\#1}$	2.1735(16)	Co2–O1	1.9218(17)
Co1–O7$^{\#2}$	2.0722(16)	Co2–O6$^{\#5}$	1.9761(18)
Co1–O8	2.0491(4)	Co2–O9	2.064(2)
Co1–O2$^{\#3}$	2.1034(16)	Co2–O2$^{\#6}$	2.3849(16)
Co1–O3$^{\#4}$	2.2224(16)	Co2–O3$^{\#7}$	1.9817(16)
Co1–O4	2.0272(17)	P1–O1	1.5077(17)
O5–Co1–O3	170.65(6)	O4–Co1–O5	86.40(7)
O7–Co1–O5	81.42(7)	O4–Co1–O7	88.58(7)
O7–Co1–O2	89.56(6)	O4–Co1–O8	95.59(8)
O7–Co1–O3	92.82(6)	O4–Co1–O2	162.94(7)
O8–Co1–O5	93.18(9)	O4–Co1–O3	86.11(7)
O8–Co1–O7	172.98(6)	O1–Co2–O6	120.07(8)
O8–Co1–O2	88.09(9)	O1–Co2–O9	99.90(8)
O8–Co1–O3	93.11(8)	O1–Co2–O2	91.95(7)
O2–Co1–O5	110.09(7)	O1–Co2–O3	120.28(8)
O2–Co1–O3	77.04(6)	O6–Co2–O9	87.30(9)

Symmetry transformations used to generate equivalent atoms: #1: 1-Y, +X-Y, +Z; #2: 1+X-Y, +X, 1-Z; #3: +Y, 1-X+Y, 1-Z; #4: 1-X, 1-Y, 1-Z; #5: 1-X+Y, +Y, 0.5-Z; #6: 1-Y, 1-X, 0.5-Z; #7: +X, 1+X-Y, 0.5-Z

MnPCF-2

Mn1–O1	1.989(2)	Mn2–O3$^{\#6}$	2.355(2)
Mn1–O2$^{\#2}$	2.236(2)	Mn2–O4	2.102(2)
Mn1–O3$^{\#3}$	2.085(2)	Mn2–O5$^{\#7}$	2.217(2)
Mn1–O7$^{\#4}$	2.113(2)	Mn2–O6$^{\#8}$	2.151(2)
Mn1–O9	2.224(3)	Mn2–O8	2.1111(8)
Mn2–O2$^{\#5}$	2.196(2)	Mn2–O3$^{\#6}$	2.355(2)
O1–Mn1–Mn2	141.87(8)	O7–Mn1–Mn2	84.51(7)
O1–Mn1–O2	103.21(9)	O7–Mn1–O2	86.88(9)
O1–Mn1–O3	125.18(10)	O7–Mn1–O9	83.03(11)
O1–Mn1–O7	116.33(11)	O9–Mn1–Mn2	122.41(8)
O1–Mn1–O9	92.93(10)	O9–Mn1–O2	163.54(9)
O2–Mn1–Mn2	43.26(6)	O2–Mn2–Mn1	44.27(6)
O3–Mn1–Mn2	47.33(6)	O2–Mn2–O3	75.77(8)
O3–Mn1–O2	80.60(8)	O2–Mn2–O5	111.27(8)
O3–Mn1–O7	118.49(10)	O3–Mn2–Mn1	40.60(5)
O3–Mn1–O9	92.82(10)	O4–Mn2–Mn1	115.02(7)

Symmetry transformations used to generate equivalent atoms: #1: +X-Y, -Y, 0.5+Z; #2: 1-X+Y, +Y, 1.5-Z; #3: -Y, -X, 1.5-Z; #4: +X, +X-Y, 1.5-Z; #5: 1-X, -Y, 1-Z; #6: -4+X-Y, -4-Y, -0.5+Z; #7: +X-Y, +X, 1-Z; #8: 1-Y, +X-Y, +Z

CoPCF-1a

Co2–O2$^{\#1}$	2.316(4)	O6–Co1$^{\#8}$	1.974(4)
Co2–O3$^{\#2}$	2.050(3)	O3–Co1$^{\#7}$	2.029(3)
Co2–O4	1.974(4)	O1–Co1	1.887(4)
Co2–O5$^{\#3}$	2.049(4)	P1–O1	1.498(4)
Co2–O7$^{\#4}$	2.011(4)	P1–O2	1.521(4)
O2–Co1$^{\#6}$	1.974(4)	P1–O3	1.550(4)
O2–Co2–Co1	42.00(9)	O5–Co2–O2	170.92(15)
O3–Co2–O2	75.02(13)	O5–Co2–O3	103.92(15)
O3–Co2–Co1	43.52(10)	O5–Co2–Co1	131.76(12)
O4–Co2–O2	82.50(15)	O7–Co2–O2	85.62(15)
O4–Co2–O3	138.10(16)	O7–Co2–O3	97.73(15)
O4–Co2–O5	103.42(16)	O7–Co2–O5	85.60(16)
O4–Co2–O7	115.49(17)	O7–Co2–Co1	70.05(11)
O4–Co2–Co1	124.48(12)	Co1–O2–Co2	86.29(14)

Symmetry transformations used to generate equivalent atoms: #1: +Y, -X+Y, 1-Z; #2: 0.33333-X+Y, 0.66667-X, -0.33333+Z; #3: 1-X, 1-Y, 1-Z; #4: 1-X+Y, 1-X, +Z; #5: +X-Y, +X, 1-Z; #6: -0.33333+Y, 0.33333-X+Y, 1.33333-Z; #7: 0.66667+X-Y, 0.33333+X, 1.33333-Z; #8: 1-Y, +X-Y, +Z

CoPCF-1'

Co1–O1	1.829(10)	Co2–O6$^{\#5}$	2.022(8)
Co1–O7$^{\#1}$	1.943(8)	Co2–O8	2.039(2)
Co1–O9	2.112(13)	Co2–O2$^{\#6}$	2.138(7)
Co1–O2$^{\#2}$	2.329(7)	Co2–O3$^{\#7}$	2.146(7)
Co1–O3$^{\#3}$	1.972(8)	P1–O1	1.513(9)
Co2–O5$^{\#4}$	2.100(8)	P1–O2	1.505(7)
O1–Co1–O7	119.9(4)	O5–Co2–O2	108.5(3)
O1–Co1–O9	97.5(5)	O5–Co2–O3	169.5(3)
O1–Co1–O2	92.7(4)	O6–Co2–O5	82.4(3)
O1–Co1–O3	129.9(4)	O6–Co2–O8	175.6(3)
O7–Co1–O9	84.0(5)	O6–Co2–O2	90.4(3)
O7–Co1–O2	87.4(3)	O6–Co2–O3	90.2(3)
O7–Co1–O3	108.9(4)	O8–Co2–O5	96.9(4)
O9–Co1–O2	169.0(5)	O8–Co2–O2	85.6(3)
O3–Co1–O9	98.3(5)	O8–Co2–O3	91.0(3)
O3–Co1–O2	78.0(3)	O2–Co2–O3	78.8(3)

Symmetry transformations used to generate equivalent atoms: #1: 1-X, 1-Y, 1-Z; #2: 1+X-Y, +X, 1-Z; #3: +Y, 1-X+Y, 1-Z; #4: 1-Y, 1+X-Y, +Z; #5: 1.33333-X, 1.66667-Y, 0.66667-Z; #6: 0.33333+X-Y, -0.33333+X, 0.66667-Z; #7: 1.33333-Y, 0.66667+X-Y, -0.33333+Z

Table S2 Comparison of surface area of some typical MOFs at 77 K and 1 atm obtained using phosphonate ligands as linker molecules ligand. Compounds containing auxiliary ligands are excluded. The respective ligand for each number in column 1 is displayed in Figure S10.

Linker	**Compound**	**Surface area**	**Space group**
1	$[Al(H_3L)(H_2O)]$	687 $m^2 \cdot g^{-1}$ (N_2, BET)	$R\bar{3}$
2	$[Cu_3(L)(H_2O)_3] \cdot 10H_2O$	647 $m^2 \cdot g^{-1}$ (N_2, BET)	*Cm*
3	$[Zr(H_4L)_2] \cdot 10H_2O$	410 $m^2 \cdot g^{-1}$ (N_2, BET)	$R\bar{3}$
4	$[Sr_2(H_2L)(CH_3OH)(H_2O)_4]$	146 $m^2 \cdot g^{-1}$ (CO_2)	$P\bar{1}$
5	$[Ni_3(L)_6 \cdot (H_2O)_6] \cdot 9H_2O$	434 $m^2 \cdot g^{-1}$ (CO_2)	$P2_1/m$
6	$H_3O[In(L)] \cdot 3H_2O$	276 $m^2 \cdot g^{-1}$ (CO_2)	*P*4/*mnc*
6	**CoPCF-1**	807 $m^2 \cdot g^{-1}$ (N_2, BET)	$R\bar{3}$
6	**MnPCF-1**	858 $m^2 \cdot g^{-1}$ (N_2, BET)	$R\bar{3}$
6	**CoPCF-2**	802 $m^2 \cdot g^{-1}$ (N_2, BET)	$P\bar{3}1c$
6	**MnPCF-1**	847 $m^2 \cdot g^{-1}$ (N_2, BET)	$P\bar{3}1c$

Table S3 Comparison of some typical MOFs for H_2 storage at 77 K and 1 atm.

Compounds	H_2 adsorption	Surface area	Refs.
CoPCF-1	1.40 wt%	815 $m^2 \cdot g^{-1}$	This work
MnPCF-1	1.30 wt%	858 $m^2 \cdot g^{-1}$	This work
CoPCF-2	1.31 wt%	802 $m^2 \cdot g^{-1}$	This work
MnPCF-2	1.27 wt%	846 $m^2 \cdot g^{-1}$	This work
UAM-150	0.85 wt%	96 $m^2 \cdot g^{-1}$	S1
UAM-151	1.05 wt%	187 $m^2 \cdot g^{-1}$	S1
UAM-152	1.60 wt%	211 $m^2 \cdot g^{-1}$	S1
MOF-74(Zn)	1.77 wt%	787 $m^2 \cdot g^{-1}$	S2
MOF-177	1.24 wt%	4526 $m^2 \cdot g^{-1}$	S2
JUC-48	1.10 wt%	880 $m^2 \cdot g^{-1}$	S2
PCN-17	0.94 wt%	820 $m^2 \cdot g^{-1}$	S2

Table S4 Comparison of CO_2 and N_2 uptake in selected metal-organic frameworks at pressures relevant to post-combustion CO_2 Capture

Compounds	CO_2 uptake at 0.15 bar (wt %)	N_2 uptake at 0.75 bar (wt %)	Temperature(K)	Selectivity(CO_2/N_2)
CoPCF-1	1.08	0.12	298	29:1
MnPCF-1	1.17	0.14	298	28:1
CoPCF-2	1.31	0.19	298	23:1
MnPCF-2	1.24	0.16	298	25:1
Ni-MOF-74[S3]	16.9	2.14	298	30:1
MOF-177[S3]	0.6	0.39	298	4:1
ZIF-100[S3]	1.0	0.15	298	22:1
$Co_4(OH)_2(doborDC)_3$	0.5	0.08	298	18:1

References

S1 E. Brunet, C. Cerro, O. Juanes, J. C. Rodríguez-Ubis and A. Clearfield, *J. Mater. Sci.* 2008, **43**, 1155-1158.

S2 M. P. Suh, H. J. Park, T. K. Prasad and D.-W. Lim, *Chem. Rev.* 2012, **112**, 782-835.

S3 K. Sumida, D. L. Rogow, J. A. Mason, T. M. McDonald, E. D. Bloch, Z. R. Herm, T.-H. Bae and J. R. Long, *Chem. Rev.* 2012, **112**, 724-781